PHILOSOPHICAL TRANSACTIONS A

rsta.royalsocietypublishing.org

Review

Cite this article: Tosoni S, Chen H-YT, Ruiz Puigdollers A, Pacchioni G. 2017 TiO_2 and ZrO_2 in biomass conversion: why catalyst reduction helps. *Phil. Trans. R. Soc. A* **376**: 20170056.
http://dx.doi.org/10.1098/rsta.2017.0056

Accepted: 21 June 2017

One contribution of 13 to a discussion meeting issue 'Providing sustainable catalytic solutions for a rapidly changing world'.

Subject Areas:
chemical physics, computational chemistry, physical chemistry

Keywords:
biomass conversion, titania, zirconia, oxygen vacancy, hydrogen spillover, oxide nanostructures, density functional theory

Author for correspondence:
Gianfranco Pacchioni
e-mail: franco.pacchioni@mater.unimib.it

TiO_2 and ZrO_2 in biomass conversion: why catalyst reduction helps

Sergio Tosoni[1], Hsin-Yi Tiffany Chen[1,2], Antonio Ruiz Puigdollers[1] and Gianfranco Pacchioni[1]

[1]Dipartimento di Scienza dei Materiali, Università di Milano Bicocca, via Cozzi 55, Milan 20125, Italy
[2]Department of Engineering and System Science, National Tsing Hua University, ESS Building, No. 101, Section 2, Kuang-Fu Road, Hsinchu 30013, Taiwan, Republic of China

Biomass refers to plant-based materials that are not used for food or feed. As an energy source, lignocellulosic biomass (lignin, cellulose and hemicellulose) can be converted into various forms of biofuel using thermal, chemical and biochemical methods. Chemical conversion implies the use of solid catalysts, usually oxide materials. In this context, reducible oxides are considered to be more active than non-reducible oxides. But why? Using density functional theory DFT + U calculations with the inclusion of dispersion forces, we describe the properties of anatase TiO_2, a reducible oxide, and tetragonal ZrO_2, a non-reducible oxide, the (101) surfaces in this context. In particular, we focus on the role of surface reduction, either by direct creation of oxygen vacancies via O_2 desorption, or by treatment in hydrogen. We show that the presence of reduced centres on the surface of titania or zirconia (either Ti^{3+} or Zr^{3+} ions, or oxygen vacancies) results in lower barriers and more stable intermediates in two key reactions in biomass catalytic conversion: ketonization of acetic acid (studied on ZrO_2) and deoxygenation of phenol (studied on TiO_2). We discuss the role of Ru nanoparticles in these processes, and in particular in favouring H_2 dissociation and hydrogen spillover, which results in hydroxylated surfaces. We suggest that H_2O desorption from the hydroxylated surfaces may be a relevant mechanism for the regeneration of oxygen vacancies, in particular on low-coordinated sites of oxide nanoparticles. Finally, we discuss the

THE ROYAL SOCIETY PUBLISHING

role of nanostructuring in favouring oxide reduction, by discussing the properties of ZrO_2 nanoparticles of diameter of about 2 nm.

This article is part of a discussion meeting issue 'Providing sustainable catalytic solutions for a rapidly changing world'.

1. Introduction

Lignocellulosic biomass represents an important raw material for the sustainable production of fuels [1]. The first step of the process consists in the pyrolysis of the lignocellulosic biomass (lignin, cellulose and hemicellulose), leading to a liquid phase which contains oxygenated organics, hydrocarbons, water, etc. [2]. The elemental composition of this bio-oil is about 56% carbon, 6% hydrogen and 40% oxygen; for comparison, a diesel fuel has an elemental composition of 90% carbon, 9% hydrogen and less than 0.3% oxygen. Therefore, in the biomass upgrading, it is essential to elongate the C-chain length and reduce the oxygen content of the raw material [3–5]. This can be achieved by means of heterogeneous catalysis processes. For instance, short-chain carboxylic acids can be condensed into heavier hydrocarbons with the elimination of water and CO_2 [3]. Heterogeneous catalysts, such as metal oxides, favour the transformation of the carboxylic acids to aldehydes or ketones [6,7]. Ketonization is a process where two carboxylic acids condense to form a ketone, eliminating H_2O and CO_2. Other condensation processes, such as aldol reaction or esterification, require the formation of an alcohol or aldehyde. Because of its importance, the mechanisms of the ketonization reaction have been investigated in detail, with particular attention paid to the role of the oxide catalyst [8–10]. A further refinement of the biofuel can occur via another catalytic step, the hydro-deoxygenation (HDO). Phenolic compounds are one of the abundant and obstinate oxygenates in the pyrolysis oil [11–13]. The reaction has been the subject of several studies [1–13]. Newman *et al*. [12] have investigated the selectivity for HDO of phenol by supported Ru catalysts. When the Ru particles are large (approx. 33 nm), the phenol molecules interact mainly with the metal particle and not with the oxide, and the reaction leads to complete hydrogenation (HYD); when Ru particles are highly dispersed (approx. 2 nm) on TiO_2 catalysts, they exhibit high selectivity and reactivity to deoxygenation of phenol to benzene.

Many catalysts have been studied for these reactions, and Ru nanoparticles supported on reducible oxides such as TiO_2 seem to offer the best performance [14]. Although the oxide catalysts (ZrO_2, TiO_2, etc.) work also without any pre-treatment, there is evidence that pre-treatment in H_2 atmosphere (oxide reduction) leads to an improved catalytic activity [8,15–17]. Interestingly, also non-reducible oxides, such as zirconia, have been used as a support catalyst in biomass upgrading [17–24]. Zirconia has been shown to be more effective in ketonization compared to other oxides widely employed in heterogeneous catalysis, such as ceria, silica or alumina [21]. Also, the phase of the oxide seems to play an important role. Monoclinic and tetragonal ZrO_2, for instance, exhibit a similar activity, not different from that of anatase TiO_2, while rutile TiO_2 is much less active [10].

These results raise some interesting questions for electronic structure theory. The first, obvious, one is why the pre-treatment in hydrogen of the catalyst results in improved conversion rates. There are several possible explanations, such as the generation of morphological changes on the surface or the presence of exposed Ti^{3+} or Zr^{3+} ions after treatment in hydrogen. According to other studies, the presence of oxygen vacancies has a beneficial effect, for instance in the ketonization of stearic acid [17]. To answer this question, we recently performed a systematic study of two reactions, the ketonization of acetic acid [25], and the HDO of phenol [26], on two catalysts consisting of tetragonal ZrO_2 (ketonization) [25], and Ru nanoparticles supported on anatase TiO_2 (HDO) [26]. In particular, we have compared the energy profiles for the two reactions on stoichiometric and reduced surfaces, assuming a low coverage of adsorbates on the surface. The results clearly show the beneficial role of the oxide reduction.

There are other open questions for theory in this topic, such as the nature of the active sites that are formed during the reduction process, the role of the supported nanoparticle, and how the treatment in hydrogen modifies the nature of the surface. This has been investigated in a series of sequential steps. First, we considered the effect of deposition of a Ru nanoparticle on the surface of a-TiO_2(101) or t-ZrO_2(101) surfaces [27]. There are cases where metal deposition on an oxide surface results in a direct electron transfer from the metal to the oxide, which becomes reduced by simple contact with the metal [28]. However, we will show that this is not the case for Ru on the two oxides under consideration. Then, we have studied the effect of exposing a Ru/TiO_2 or a Ru/ZrO_2 catalyst to H_2, in order to study whether hydrogen dissociation occurs, and how hydrogen adsorption modifies the electronic structure of the oxide [29]. In this study, particular attention has been given to the progressive increase in hydrogen loading, until saturation coverage is reached. The results elucidate how, in the presence of a supported metal particle (Ru in this case), exposure to hydrogen leads to a hydroxylated surface. The next step has been to consider water desorption from the hydroxylated surface, with the formation of oxygen vacancy. This is a key step for the catalytic generation of oxygen vacancies, which is necessary to produce a significant change in the activity of the catalyst.

The last aspect to be addressed by theory is the difference between titania and zirconia as supports for the reaction. While TiO_2 is a reducible oxide, with relatively low formation energy of oxygen vacancies, zirconia is hardly reducible, with high oxygen vacancy formation energies [30]. On this basis, one should expect a rather different behaviour of the two oxides. In this context, we have examined the reducibility of zirconia as a function of nanostructuring [31,32]. We have studied the cost of removing oxygen, or the effect of adding hydrogen, as a function of the dimension of zirconia nanoparticles. The results show the existence of a very important effect of nanostructuring on the final properties of the oxide support.

The paper is organized as follows. In §2, we give the essential information about the calculations performed. Section 3 shows how the presence of reduced centres on the surface of titania or zirconia (either Ti^{3+} or Zr^{3+} ions or oxygen vacancies) results in lower barriers and stable intermediates in two key reactions in biomass catalytic conversion: ketonization (studied on ZrO_2) and phenol deoxygenation (studied on Ru/TiO_2). Having established the positive role of oxide reduction in two key catalytic processes, in §4 we address the mechanisms that can lead to surface reduction. In §4a, we discuss the role of depositing a small Ru cluster on the surfaces of a-TiO_2 and t-ZrO_2; in §4b, we consider the role of pre-treatment in H_2, from hydrogen dissociation to hydrogen spillover and reverse spillover; in §4c, we discuss reduction by H_2O desorption from a hydroxylated surface. Section 5 is dedicated to analyse the role of nanostructuring, and is restricted to results obtained on ZrO_2. We first consider the cost of formation of oxygen vacancies, §5a, and then the mechanism of H_2 dissociation, §5b, on zirconia nanoparticles. Finally, some general conclusions are summarized in §6.

2. Computational details

All the calculations have been performed with the VASP 5.3 simulation package [33]. The electronic structure is calculated using the PBE (Perdew–Burke–Ernzerhof) exchange–correlation functional [34]. To improve the description of the electronic structure of titania and zirconia, partial occupations of Ti and Zr d orbitals are penalized by a Hubbard parameter, which has been empirically set to 3 eV for Ti and 4 eV for Zr (generalized gradient approximation GGA + U approach) [35,36]. The long-range dispersion interactions are added according to the density functional theory DFT + D2′ semi-empirical approach. This scheme slightly modifies the original parametrization proposed in the DFT + D2 method by Grimme [37]. As recently shown [38], this approach provides reasonably accurate results in describing oxide surfaces when compared with more complex and resource-intensive methods, such as the van der Waals density functionals.

Valence electrons, i.e. H(1s), C and O(2s, 2p), Ti(3s, 4s, 3p, 3d) and Zr(4s, 5s, 4p, 4d), are expanded on a set of plane waves with a kinetic cut-off of 400 eV, while core regions are treated

with pseudo-potentials, as encoded in the projector augmented wave approach [39,40]. Further details can be found in refs. [25–27,29,31,32].

3. Effect of oxide pre-reduction on reactivity

(a) Ketonization on ZrO_2

Metal oxides are commonly used to catalyse the transformation of the carboxylic acids to aldehydes or ketones [6–16]. A stepwise mechanism implying the formation of a β-keto acid intermediate [21,41] is considered as dominating in the ketonization reaction. The elementary steps of the mechanism, α-hydrogen abstraction and C–C coupling, are depicted in figure 1. These are followed by C–C scission with CO_2 formation and enolate HYD to form acetone (not shown). In step (*a*), an acetic acid molecule is adsorbed on zirconia, forming an acetate ion and a hydroxyl group grafted on the surface. The adsorbed acetate ion is further subjected to the enolization reaction (step (*b*1)), where a proton from the methyl group is transferred to the surface, forming a hydroxyl and a 1,1-ene-diolate species (intermediate 1). Alternatively (step (*b*2)), the acetate molecule undergoes deoxygenation, forming an acyl species (intermediate 2) and an OH^- group bound to a surface cation. In step (*c*), the enolate and acyl intermediates 1 and 2, respectively, combine to form a β-keto acid ion, namely the 3-oxo-butyrate in the case of acetic acid reaction.

The ketonization of carboxylic acids on anatase and rutile TiO_2 and monoclinic and tetragonal ZrO_2 has been considered recently in a very detailed and extended theoretical–experimental study by Wang and Iglesia [10]. The main conclusion of this work is that ketonization turnover rates are much higher on m-ZrO_2, t-ZrO_2 and a-TiO_2 than on r-TiO_2; the reason lies in the particular cation–cation distances that stabilize the bidentate bonding mode of acetate compared to the monodentate species. At very high coverages, in fact, the less stable monodentate acetate ion becomes the key reactive intermediate, while the more stable bidentate molecules only act as spectators [10]. In this work, it was also shown that pre-treatment in H_2 of a-TiO_2 at 543 K did not result in changes in ketonization rates, indicating that either reduced centres do not form during the treatment or that they do not play a role in the reaction. This is different from what was reported by Pham *et al.*, who showed that the ketonization activity increases with a reductive pre-treatment of a Ru/TiO_2 catalyst, and it drops when the reduced catalyst is exposed to O_2 before the reaction [8,15]. This could be interpreted as an essential role of the supported metal particle in the reduction process, consistent with the results presented here about hydrogen spillover (see below). It is also possible that the role of reduced centres is important at low coverages of carboxylic acids, while at high coverage geometrical effects dominate over electronic effects associated with reduction.

The reaction path has been analysed by means of DFT + U calculations, comparing the properties of defect-free and defect-rich ZrO_2(101) (reduced) surfaces [25]. Reduced centres on the zirconia supports are modelled by considering (a) hydrogenated surfaces or (b) oxygen-deficient surfaces, ZrO_{2-x}. There is a substantial difference between these two situations. On reducible oxides, treatment in hydrogen results in an adsorbed proton (OH group) and an excess electron that reduces a M^{4+} ion to M^{3+} without implying a change in the morphology of the surface (except for the appearance of the OH group). Oxygen removal, on the other hand, results in both a morphological defect (oxygen vacancy) and an electronic modification due to the formation of trapped electrons. While these two situations can be distinguished by theory, they are more difficult to access experimentally.

For the calculations, a single acetic acid molecule has been considered, thus modelling low-coverage situations. The results show that on non-reduced t-ZrO_2, the reaction of the acetate ion to give the enolate intermediate is hindered by rather large activation energy, similar to that reported for the same reaction on monoclinic zirconia at the PBE level [42]. On the stoichiometric surface, the deoxygenation of the acetate fragment is even more unfavourable, because the acylium cationic intermediate is unstable and tends to abstract one oxygen ion from the surface, reforming acetate. In short, the regular surface appears as only moderately active or even inactive.

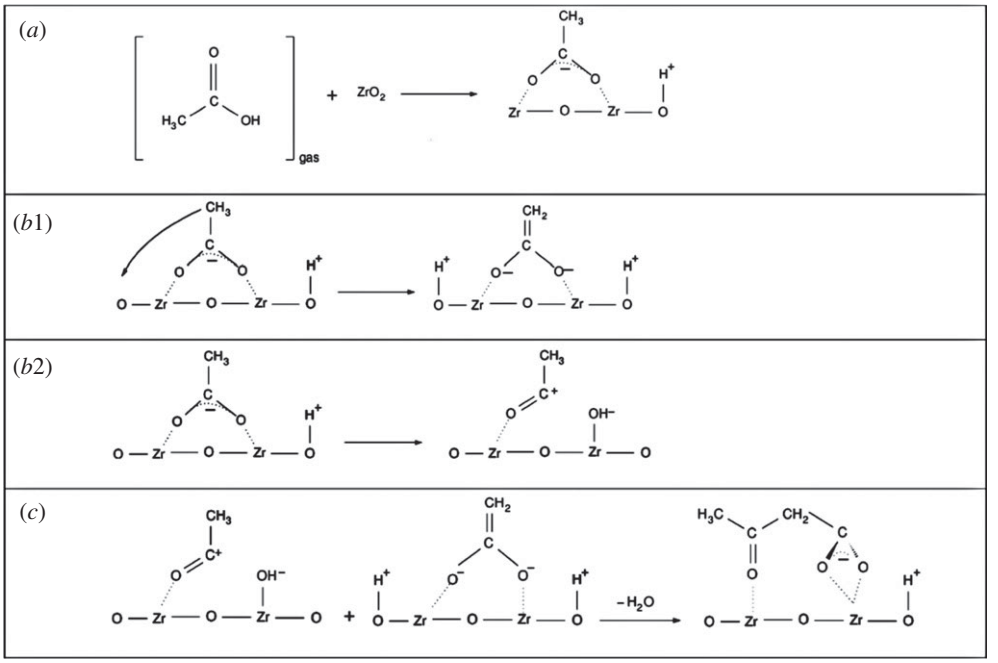

Figure 1. Ketonization on the zirconia surface: (*a*) adsorption of acetic acid, (*b*1) formation of the enolate intermediate 1, (*b*2) formation of the acyl intermediate 2, and (*c*) reaction of acyl and enolate to form the β-keto acid. Reproduced from ref. [25]. Copyright © 2016 Elsevier.

Completely different is the behaviour of the reduced surface. If the reduction occurs by H addition (see below) one can assume the formation of an OH group and a Zr^{3+} ion. The electron associated with this reduced centre is easily transferred to the acetate ion during the deoxygenation reaction, forming an acyl radical, which easily reacts with the enolate fragment to form the β-keto acid. This shows that exposed Zr^{3+} ions, if present, can be extremely beneficial for the ketonization reaction. Also the presence of a surface oxygen vacancy has a strong impact on the keto–eno tautomeric equilibrium, where the enolate species is strongly stabilized with respect to the acetate fragment. The kinetic barrier is considerably smaller compared to stoichiometric zirconia. Similarly, in the deoxygenation step, one also observes a remarkable stabilization of the reaction intermediate in the form of an anionic acyl species. The combination of enolate and acyl ions to form the β-keto acid is therefore easier than on the stoichiometric surface. These results clearly show the beneficial role of zirconia surface reduction for the low-coverage ketonization reaction.

Clearly, in a catalytic process, the reactive centres need to be regenerated in the course of the reaction. Zr^{3+} centres can be created by the initial pre-treatment of the catalyst in hydrogen and can be regenerated after the reactants have transformed into products. More complex is the regeneration of oxygen vacancies. One possible scenario is that they are produced thanks to the presence of water (in humid environment the catalyst surface is hydroxylated). The calculations show that at the temperatures of the reaction, around 600 K, water can start to desorb from the surface, leaving behind oxygen vacancies, in particular corresponding to low-coordinated sites. This will be further discussed in §4c.

In summary, the calculations show that, while it is not essential to reduce the zirconia surface (the reaction can occur also on stoichiometric surfaces), pre-reduction has the overall effect of lowering the barriers and stabilizing some key intermediates, making the reaction easier [25], at least in the limit of low coverage of adsorbed species.

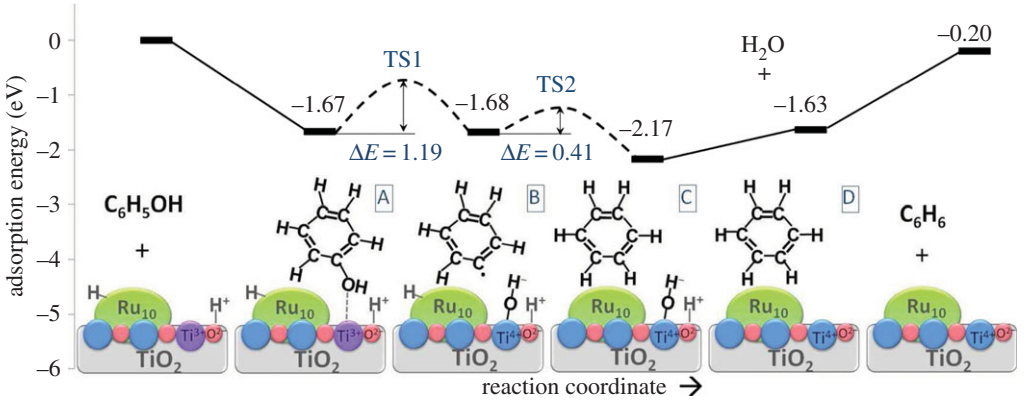

Figure 2. Reaction of phenol (C_6H_5OH) on anatase (101) surface with one H adsorbed on Ru_{10} and one H adsorbed on the oxide (Ti^{3+} centre). Energies in eV. Reproduced from ref. [26]. Copyright © 2016 John Wiley and Sons. (Online version in colour.)

(b) Direct deoxygenation on TiO_2

The HDO mechanism of phenol is a relevant step in the treatment of biomass to generate biofuels [11–13]. It can occur according to two main pathways: (i) HYD followed by dehydration; and (ii) direct deoxygenation (DDO). Our scope is to compare the reactivity of phenol adsorbed on Ru_{10} clusters deposited on stoichiometric and reduced anatase TiO_2(101) surfaces. We have restricted our analysis to the DDO reaction and we concentrate on the interface region between the oxide and the metal particle. In particular, we have studied the DDO of phenol via breaking of the C–OH bond and oxygen removal. The assumption is that Ru nanoparticles of size below 1–2 nm are present on the surface. In fact, the surface of large Ru particles is very active and leads to C–OH bond scission with similar and even lower energy barriers [12]. In this case, it is assumed that, in the presence of hydrogen, the reaction proceeds towards full HYD. In analogy with the study of ZrO_2 in the ketonization process, see above, three different forms of anatase TiO_2 have been considered: (i) the ideal stoichiometric (101) surface; (ii) the same surface reduced by H addition and formation of Ti^{3+} radical ions; and (iii) the surface with one O vacancy and two Ti^{3+} centres.

We found that on the surface reduced by hydrogen addition (Ti^{3+} ions), the phenol molecular and dissociative adsorptions ($C_6H_5 + OH$ fragments) become isoenergetic, and the barrier to dissociate the C–OH bond is 1.19 eV, indicating a possible channel for deoxygenation of phenol, figure 2.

On the surface reduced by O vacancies, the dissociative adsorption is 0.22 eV more stable than the molecular adsorption, indicating a thermodynamically slightly favourable process; the C–OH activation energy, however, is higher, 1.50 eV. The results show that the C–O scission can be an important step towards DDO. The final step, benzene desorption, costs about 1.4 eV, an energy which is similar to the barrier implied in the O removal from the phenol molecule. In both cases, the role of the reduced surface is important as well as that of the metal/oxide interface. In this respect, the DFT calculations are consistent with the mechanism of deoxygenation of phenol on Ru/TiO_2 proposed by Newman *et al*. [12].

4. Mechanisms of surface reduction

In figure 3, we report the density of states (DOS) curves of a-TiO_2(101) and t-ZrO_2(101) surfaces. The TiO_2 surface displays a band gap of 2.6 eV; the bulk value, 2.4 eV, is underestimated with respect to the experiment, 3.2 eV. The band gap of the t-ZrO_2(101) surface (3.8 eV) is smaller than that calculated for the bulk (4.5 eV; electron energy loss spectroscopy gives 4.2 eV [43] while vacuum ultraviolet absorption spectroscopy measurements give values between 5.8 and 6.6 eV [14]). The alignment of the energy levels with respect to vacuum, figure 3, allows one to

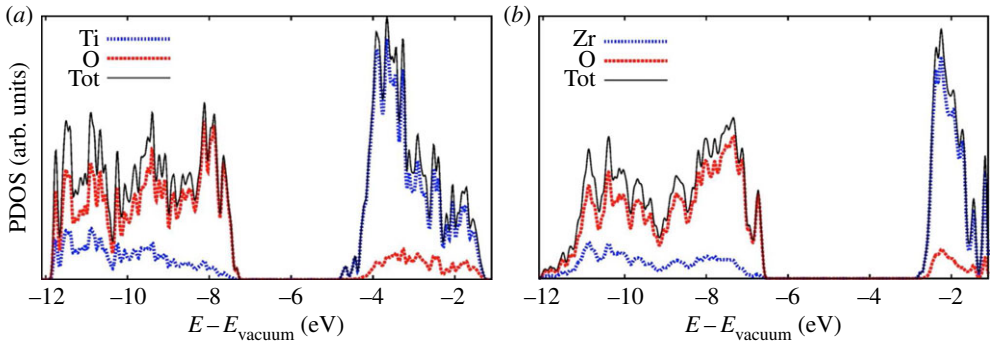

Figure 3. Total and projected DOS of (101) surfaces of (*a*) a-TiO_2 and (*b*) t-ZrO_2. Energies with respect to the vacuum level set to zero. Reproduced from ref. [27]. Copyright © 2014 American Chemical Society.

directly compare the positions of the bands of the two surfaces. This is important information to rationalize the behaviour of supported metal particles on the two oxides. The edges of both occupied and virtual states of TiO_2 lie at lower energy compared to those of ZrO_2. The top of the valence band (VB) in a-TiO_2(101) is calculated at −7.3 eV, while it is at −6.6 eV eV in t-ZrO_2(101). The bottom of the conduction band (CB) on a-TiO_2(101) is at −4.7 eV, whereas in t-ZrO_2(101) it is at −2.8 eV [27]. These results are consistent with TiO_2 being easier to reduce (lower CB minimum) and harder to oxidize (lower VB maximum) than ZrO_2.

(a) Deposition of Ru clusters

It has been found experimentally that the ketonization rate can be enhanced by adding metal particles, such as Ru, on the surface of the oxide catalyst [14–16]. The role of the metal in enhancing the activity of the catalyst is still a matter of debate. It has been suggested that the addition of Ru helps to enhance the reducibility of TiO_2 and that this should result in the easier formation of coordinatively unsaturated Ti^{3+} sites [14]. A similar effect has been suggested for ZrO_2 due to the presence of Zr^{3+} ions [44,45]. The problem has been investigated by studying the adsorption of Ru_1 (atoms) and Ru_{10} (clusters) on the most stable (101) surfaces of both TiO_2 and ZrO_2 oxides to identify the nature of the interaction of the metal with the support and to compare the behaviour of the two oxides [27].

The theoretical study of metal clusters on a supporting oxide surface is complicated by the presence of several minima. We used a model consisting of a Ru_{10}(7,3) two-layer cluster. This structure has a larger metal-oxide interface (seven atoms), that favours the adhesion of the cluster to the support, and a second layer of three metal atoms exposed to the vacuum region. A 10-atom cluster is small enough to belong to the so-called non-scalable regime of properties, where quantum size effects play an important role. In this respect, the results have qualitative more than quantitative character. The Ru_{10}(7,3) cluster has been optimized both in the gas phase and on a-TiO_2(101) and t-ZrO_2(101) supports.

On a-TiO_2 Ru_{10}(7,3) is bound on O_{3c} sites ($E_{ads} = -5.99$ eV). A more stable isomer is strongly distorted and classified as Ru_{10}(6,4), with $E_{ads} = -6.94$ eV, table 1. The Bader charge of both Ru_{10} clusters is 1.2–1.3 $|e|$, suggesting the occurrence of an electron polarization from Ru_{10} to the TiO_2 surface, consistent with previous work [46,47]. However, no evidence of the formation of Ti^{3+} ions is found even after artificial distortion of the lattice to favour the formation of the small polaron around the Ti^{3+} centre. This clearly indicates that the Ru_{10} cluster is bound to TiO_2 mainly via Ru–O covalent polar bonds without the occurrence of a net charge transfer. In this respect, Ru_{10} does not induce a reduction of the oxide surface. Things are completely different when, for instance, an alkali metal is deposited on the surface, as this clearly results in the formation of reduced Ti^{3+} ions [48].

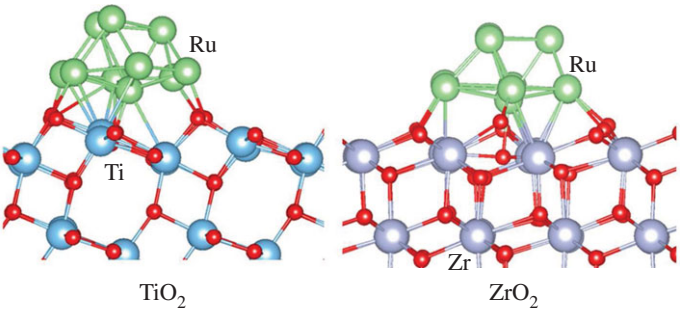

Figure 4. Left: Ru_{10} cluster adsorption on a-TiO_2(101). Right: Ru_{10} cluster adsorption on t-ZrO_2(101). (Online version in colour.)

Table 1. Adsorption energy, E_{ads}, number of unpaired electrons, $N_\alpha - N_\beta$, and Bader charge, q, of Ru_{10} adsorbed on stoichiometric a-TiO_2(101) and t-ZrO_2(101) surfaces.

			$N_\alpha - N_\beta$		q (Ru_{10})
	supercell	E_{ads} (eV)	Ru_{10}	MO_2	$\|e\|$
a-TiO_2	$Ti_{60}O_{120}/Ru_{10}$(7,3)	−5.99	+1.9, −1.9	−0.1	+1.18
	$Ti_{60}O_{120}/Ru_{10}$(6,4)	−6.94	2.8	0.3	+1.28
t-ZrO_2	$Zr_{60}O_{120}/Ru_{10}$	−8.49	+1.9, −0.1	0.0	+0.28

A similar procedure has been followed for Ru_{10} on t-ZrO_2. The central Ru atom in the bottom layer of Ru_{10} has been placed on the top of O or on the top of Zr, with the former clearly more stable. The adsorption energy of Ru_{10} on the top of O, −8.49 eV, is considerably higher than that of the corresponding isomer on a-TiO_2 (−5.99 eV), table 1.

A major structural rearrangement occurs on the ZrO_2 surface upon deposition of Ru_{10}, at variance with anatase. The O_{3c} atom below the cluster moves down, figure 4; this local rearrangement results in an almost undistorted Ru_{10} cluster compared to the gas-phase isomer, figure 4. The strain at the metal–oxide surface is distributed on the oxide and not on the metal. The Bader charge on the entire cluster is much smaller than in the TiO_2 case, 0.28 $|e|$ (table 1), and there is no evidence of formation of Zr^{3+} ions, indicating that there is no direct reduction of the oxide surface by deposition of Ru_{10}.

The main objective of this part of the investigation is to verify if a Ru nanoparticle deposited on the oxide surface induces a net charge transfer, with consequent reduction of the oxide, as found for other systems, such as Ag nanoparticles deposited on CeO_2 [49]. The results, however, rule out this possibility. For ZrO_2, we have no evidence of the formation of Zr^{3+} ions when Ru atoms or clusters are deposited on the surface. This is consistent with the fact that TiO_2 is more reducible than ZrO_2. However, the general conclusion is that direct reduction of the TiO_2 or ZrO_2 supports does not occur by simple deposition of the Ru metal.

We have also considered an alternative process, reduction of the oxide by the effect of an oxygen reverse spillover. In fact, in the presence of a metal nanoparticle, O atoms may diffuse from the oxide surface to the metal, leaving behind an oxygen vacancy, with consequent reduction of the oxide. This is the initial step of what is often referred to as strong metal–support interaction. The thermodynamic cost to displace an O atom from the (101) surface of TiO_2 and ZrO_2 in the presence of a Ru nanoparticle has been estimated: it is very small, about 0.2 eV, on TiO_2, and moderate, about 0.6 eV, on ZrO_2. On the regular zirconia surface the process is associated with a rather high barrier. Moving an O atom from the Ru/ZrO_2 interface to the first layer of the Ru_{10} cluster costs 1.74 eV. Smaller barriers, of 0.3 eV, are required for the O atom to diffuse to the most stable adsorption site on the top layer of the Ru_{10} cluster. In general, the formation of

O vacancies on oxide surfaces is lower on steps, edges and other defects, which are particularly abundant on oxide nanoparticles [50,51]. A reduction of the formation energy of the O vacancy by about 0.5 eV on a low-coordinated site would result in an exothermic O reverse spillover on TiO_2 and an almost thermoneutral process on ZrO_2. In this respect, the oxygen reverse spillover is a mechanism of potential interest for the reduction of the oxide surface in reducing conditions. However, the barriers for oxygen migration are relatively high and they may hinder the process kinetically.

(b) Hydrogen spillover

Hydrogen pre-treatment results in an increased activity of oxide catalysts such as TiO_2 and ZrO_2 for the production of biofuels from cellulose-based biomass [8,15–17]. Hydrogen spillover occurs from metal particles (Ru in our case) to the supporting oxide surface (TiO_2 or ZrO_2):

$$H_2 + Ru/MO_2 + 2O^{2-}_{MO_2} \rightarrow 2H/Ru/MO_2 + 2O^{2-}_{MO_2} \rightarrow Ru/MO_2 + 2OH^{-}_{MO_2} + 2e^{-} \tag{4.1}$$

For a long time, the assumption has been that hydrogen spillover does not take place on non-reducible oxides, and the question has been highly debated [52]. A recent experiment provides a convincing answer [53]. Comparing Pt nanoparticles on TiO_2 (reducible) and Al_2O_3 (non-reducible) supports, it has been demonstrated that hydrogen spillover occurs on both surfaces but with different efficiencies. On alumina the process is 10 orders of magnitude slower than on titania and is restricted to very short distances from the supported Pt particles.

The spontaneous occurrence of the opposite phenomenon, i.e. hydrogen reverse spillover, is also possible [54–57]. In this case, the hydrogen atom from an OH group of the oxide surface migrates to the supported metal particle. Under operating conditions, the occurrence of the direct or reverse hydrogen spillover depends on the hydrogen partial pressure. By changing this parameter, one changes the hydrogen chemical potential and the direction of the equilibrium.

If direct hydrogen spillover occurs, with migration of hydrogen from the metal particle to the oxide, then the final situation is formally analogous to the direct adsorption of H_2 on the oxide surface. When two H atoms are added to the bare MO_2 surface (M = Ti or Zr), they form hydroxyl groups:

$$H_2 + 2O^{2-}_{MO_2} + 2M^{4+}_{MO_2} \rightarrow 2OH^{-}_{MO_2} + 2M^{3+}_{MO_2} \tag{4.2}$$

The electron associated with atomic H is transferred to a metal cation, which changes its oxidation state from M^{4+} to M^{3+} (oxide reduction [58]). This opens the question about the nature of the species that diffuses from the metal particle: a neutral H with its valence electron, or a proton? In the first case one electron is transferred from the metal particle to the oxide, with its consequent reduction; in the second case the electron remains on the metal, which carries a negative charge, and no direct reduction of the oxide occurs. We have compared the process for Ru clusters supported on TiO_2 and ZrO_2.

Neither TiO_2 nor ZrO_2 surfaces are able to spontaneously split the H_2 molecule with the formation of two surface OH groups and two electrons (homolytic dissociation). On titania the cost is rather small, 0.13 eV, while on zirconia it is much higher, 1.69 eV. On ZrO_2, the formation of an isolated surface OH group by H atom adsorption has a cost of 0.79 eV, computed with respect to $\frac{1}{2}H_2$. This is not exactly half the energy of adsorbing an H_2 molecule due to some mutual repulsion phenomena on the surface. The formation of a hydroxyl group is accompanied by a transfer of the H valence electron to a Ti 3d or Zr 4d empty state at the bottom of the oxide CB. Since the CB in ZrO_2 is higher than in TiO_2 (see §4), the process is less favourable. Indeed, on ZrO_2 the most stable dissociation state of H_2 is not homolytic (formation of two OH groups and two Zr^{3+} ions), but heterolytic, with the formation of a proton, H^+, bound to a surface O^{2-} atom (OH group), and a hydride ion, H^-, bound to a Zr^{4+} cation. This is typical of non-reducible oxides, like MgO [59].

As mentioned above, the homolytic mechanism implies an electron transfer from the hydrogen molecule to the Zr 4d empty states. It is worth noting that the energetics associated with this

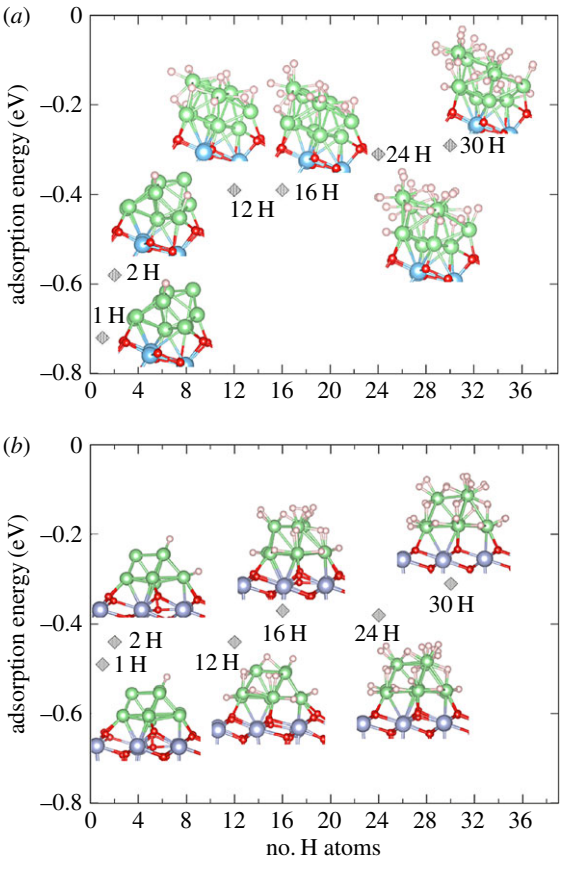

Figure 5. Calculated average adsorption energy per adsorbed H atom, computed as $[E(Ru_{10}(H_n)/MO_2) - E(Ru_{10}/MO_2) - n/2\,E(H_2)]/n$, against number of H atoms on Ru_{10}/TiO_2 (*a*) and Ru_{10}/ZrO_2 (*b*). The structure of the hydrogenated clusters is shown in the insets. Reproduced from ref. [29]. Copyright © 2015 American Chemical Society. (Online version in colour.)

process strongly depend on the adopted computational scheme. With bare PBE, for instance, the energy necessary for the homolytic splitting drops from +1.69 eV to +0.64 eV. The reason is that the PBE method severely underestimates the band gap of zirconia, which reflects also in an underestimation of the energy necessary to create Zr^{3+} centres.

A comparison of the adsorption of an H atom on either the O sites of TiO_2 or ZrO_2, or the Ru sites of the cluster, shows unambiguously that this latter is the preferred situation. H adsorbs preferentially on Ru_{10}, forming strong Ru–H bonds with hydride character. A spontaneous, non-activated, dissociation of the H_2 molecule occurs on the Ru cluster whose role is to split hydrogen and to bind a large amount of H atoms. Up to three H atoms can be added per Ru atom in the cluster, with an overall exothermic reaction, figure 5, in agreement with other estimates (e.g. for H on Pt [60]). This clearly shows that the role of the Ru_{10} cluster is to split the H_2 molecule in a barrierless process and to generate isolated H atoms that can diffuse to the oxide surface once saturation coverage on the cluster has been reached, figure 5.

In fact, direct spillover of hydrogen from the Ru particle to the oxide surface is unfavourable at low hydrogen coverage. Two H atoms on the Ru cluster are 0.3–0.4 eV more stable than one H atom on the metal and the other on the oxide. The cost to displace H from Ru to the oxide, however, decreases gradually as more hydrogen is adsorbed on the metal cluster. At a coverage of about 30 H atoms on Ru_{10}/TiO_2, it becomes thermodynamically favourable to move one H from the metal to the oxide. On zirconia the situation is similar, but the effect appears already for a coverage of 24 H atoms. We also estimated the barrier for the diffusion of an H atom from the

metal particle to the TiO_2 surface. This is about 0.4 eV, very close to that reported recently for the same process in a different study, 0.45 eV [53].

Previous studies on hydrogen diffusion on the anatase TiO_2(101) surface have shown that hydrogen preferentially diffuses into the bulk compared to the surface, and that the smallest barrier for surface-to-bulk diffusion is of about 0.7 eV [53,61]. Our calculations indicate a barrier for surface diffusion of about 0.7 eV (see below). Thus, the barrier for H diffusion on the titania surface is higher than that required to diffuse an H atom from the Ru cluster to the oxide surface.

From an electronic point of view, the addition of a single H atom to TiO_2 or ZrO_2 leads to the reduction of the two oxides with the formation of Ti^{3+} $3d^1$ and Zr^{3+} $4d^1$ centres. This gives rise to localized electrons in the material. The occurrence of a chemical reduction of the oxide by hydrogen addition or by hydrogen spillover is clearly shown by the net atomic charges. In particular, when an H atom migrates from the Ru_{10} particle to TiO_2 or ZrO_2, the nuclear motion is accompanied by a charge flow from the metal to the oxide. Note, however, that things are different on the bare surface of zirconia when more than one H is adsorbed. In this case, in fact, the preferred situation is that corresponding to the formation of a proton and a hydride ion (heterolytic mechanism). This is because a hydride ion bound to Zr^{4+} has its levels at lower energy than the Zr 4d states.

These theoretical results shed light at the atomistic level on the mechanism of hydrogen spillover and are fully consistent with experimental observations. For instance, Panayotov and Yates [62] demonstrated in a study of hydrogen spillover on Au/TiO_2 that the rate of spillover is proportional to $P_{H_2}^{1/2}$, indicating that the H atoms originate from the equilibrium dissociative adsorption of H_2 on the Au particle. Furthermore, the diffusion of H atoms into the oxide is accompanied by the formation of trapped electrons in shallow trap states near the bottom of the CB edge [62]. Also the recent experimental–theoretical work of Karim *et al*. [53] is fully consistent with the present conclusions.

(c) Water desorption from hydroxylated surfaces

The cost of formation of an oxygen vacancy on the surface of t-ZrO_2 (computed with respect to $\frac{1}{2}O_2$) is about 6 eV [31]; this value does not change significantly if one considers low-coordinated O atoms at steps [31]. Lower formation energies have been computed for a-TiO_2 (4.45 eV [27]), in agreement with a more reducible nature of this oxide. O vacancies can also be formed starting from a hydroxylated surface, and removing H_2O. This has been considered for both a-TiO_2(101) and t-ZrO_2(101) surfaces.

Let us consider TiO_2 first. The overall reaction is $TiO_2 + 2H \rightarrow TiO_{2-x} + H_2O$. Once the surface is hydroxylated (see §3b), the two H atoms need to migrate in order to become close to each other, figure 6. This process has a barrier of about 0.7 eV [61]. By overcoming a second barrier of 0.3 eV, the two H atoms become bound to the same O ion, forming the precursor state for water dissociation. The removal of a water molecule costs 1.20 eV, so that the entire cost to create a vacancy starting from the hydroxylated TiO_2 surface is 1.79 eV, figure 6. This is much lower than that associated with O removal via formation of $\frac{1}{2}O_2$ (4.45 eV [27]). Using a Redhead equation for first-order desorption processes [63,64], $\Delta E_{des} = RT_{des}(\ln \nu T_{des} - 3.64)$, a standard pre-factor $\nu = 10^{13}\,s^{-1}$ and a barrier of 1.2 eV, one can conclude that thermal desorption of water is possible for temperatures around 450 K, below the temperatures involved in many catalytic processes, figure 6. Lower formation energies are expected corresponding to low-coordinated sites present on oxide nanoparticles.

We consider now the same process on ZrO_2, figure 7. The heterolytic splitting of H_2 is slightly exothermic (−0.06 eV) (much lower than the energy associated with the homolytic splitting, +1.69 eV, see above). The formation of an adsorbed water molecule starting from the hydroxylated surface is highly endothermic (+2.47 eV) and implies a barrier as large as 3.33 eV, figure 7. Once the precursor state has been obtained, the water molecule can desorb in the gas phase with a cost of 1.10 eV, similar to TiO_2 (1.2 eV). This process generates a neutral oxygen

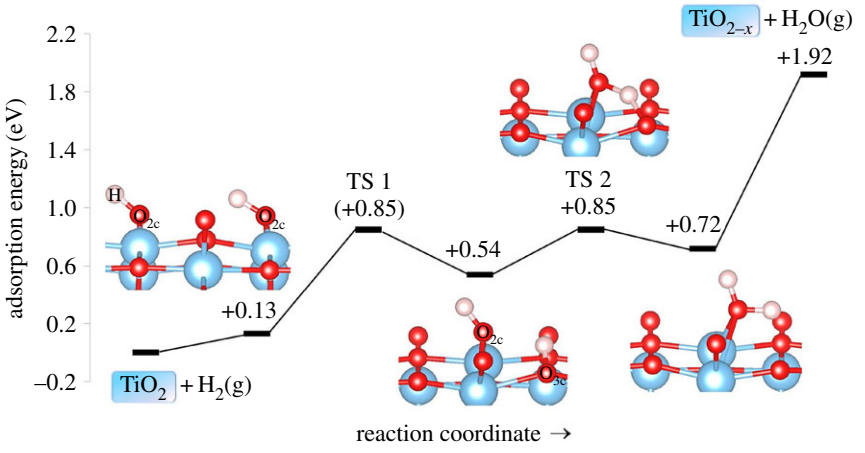

Figure 6. Reaction scheme for the formation of an O vacancy on the hydroxylated anatase (101) surface via water desorption. Energies in eV. 3 × 1 supercell calculations. Blue, Ti; red, O; white, H. Reproduced from ref. [26]. Copyright © 2016 John Wiley and Sons. (Online version in colour.)

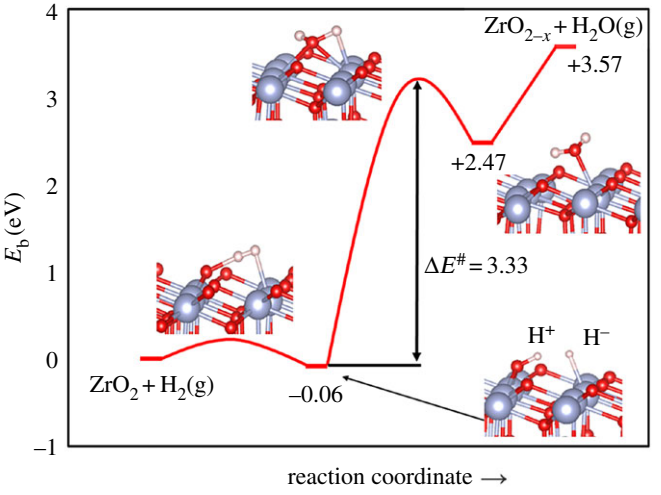

Figure 7. Energy profile for HYD, formation of adsorbed water, and water desorption with creation of a surface oxygen vacancy on the t-ZrO_2(101) surface. Blue, Zr; red, O; white, H. Energies in eV. Reproduced from ref. [25]. Copyright © 2016 Elsevier. (Online version in colour.)

vacancy on the surface of t-ZrO_2, figure 7. The final enthalpy cost of O vacancy formation via water desorption starting from the hydroxylated surface, 3.57 eV, is still very high, but much lower than that computed for O removal via O_2 desorption, about 6 eV. These values need to be corrected by entropy contributions. Assuming $T = 573$ K, we obtain a $T\Delta S_{des}$ contribution of −0.85 eV, which results in a $\Delta G_{des} = 2.72$ eV [25]. Again, this cost could be further reduced if one considers zirconia nanoparticles instead of the regular (101) surface.

5. Oxide reducibility: role of nanostructuring

In this section, we consider a particular aspect of oxide reducibility, related to nanostructuring. In particular, we will concentrate on a single oxide, zirconia, a poorly reducible material when in the bulk form. We will consider the effect of generating zirconia nanoparticles on two properties:

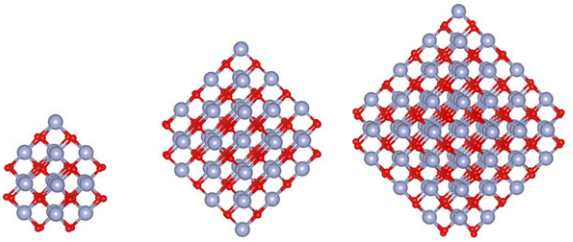

Figure 8. Models of partly truncated octahedral stoichiometric zirconia nanoparticles $(ZrO_2)_n$. Zr is represented by big blue atoms and O by small red atoms. (Online version in colour.)

Table 2. Formation energies, in eV, of *n*-coordinated O_{nc} – vacancies of partly truncated octahedral (ZrO_2 stoichiometric) zirconia nanoparticles and the (101) surface of t-ZrO_2.

system	corner – O_{2c}	corner – O_{3c}	facet – O_{3c}	inner – O_{4c}
t-ZrO_2(101) surface	–	–	+5.97	+5.67
$Zr_{16}O_{32}$	+3.94	–	+5.89	+5.15
$Zr_{40}O_{80}$	+3.70	+4.16	+4.86	+5.11
$Zr_{80}O_{160}$	+2.62	+5.26	+4.42	+2.17

(i) the cost of oxygen removal (formation of O vacancies) [31]; and (ii) the effect of reducing the oxide by the addition of H_2 molecules [32].

(a) Oxygen removal from Zr_xO_{2x} nanoparticles

By cleaving t-ZrO_2 along the O-terminated {101} surfaces, we generated octahedral $Zr_{19}O_{32}$, $Zr_{44}O_{80}$ and $Zr_{85}O_{160}$ nanoparticles. These nanoparticles are not stoichiometric; in particular, they are highly oxygen deficient. To restore the ZrO_2 stoichiometry, three, four and five Zr corners, respectively, were cut from the octahedral structures, resulting in the chemically stoichiometric $Zr_{16}O_{32}$, $Zr_{40}O_{80}$ and $Zr_{80}O_{160}$ systems (partly truncated octahedral nanoparticles, figure 8) [31]. The maximum diameters (between nuclei of opposite Zr corner atoms) are 0.90, 1.40 and 1.92 nm; note that considering atomic radii will result in even larger sizes.

We computed the formation energy of the O vacancies in the nanoparticles, taking $\frac{1}{2}O_2$ as a reference, table 2. The values are compared to those calculated for the extended t-ZrO_2(101) surface. O vacancies are easier to form corresponding to the low-coordinated O_{2c} and O_{3c} sites, table 2. We go from the nearly 6 eV required to remove O from the (101) surface, to the 2.62 eV needed to remove a corner O_{2c} atom from $Zr_{80}O_{160}$. On the other hand, the cost to create O_{4c} vacancies in the inner part of the $Zr_{16}O_{32}$ and $Zr_{40}O_{80}$ nanoparticles does not change significantly compared to the O sites with the same coordination in the extended (101) surface; only for the larger $Zr_{80}O_{160}$ particle do the inner O_{4c} vacancies have a much lower formation energy due to geometry relaxation effects. One can conclude that the surface O_{2c} and O_{3c} sites in the nanoparticles represent important reactive centres in O-transfer redox reactions; nanostructuring has a significant effect on the reducibility of zirconia, enhancing its catalytic activity with respect to the extended surfaces.

(b) Hydrogen addition to Zr_xO_{2x} nanoparticles

We have seen above that H_2 prefers to dissociate on the regular ZrO_2(101) surface through a heterolytic mechanism in which $Zr–H^-$ and $O–H^+$ bonds are formed. This is the classical H_2

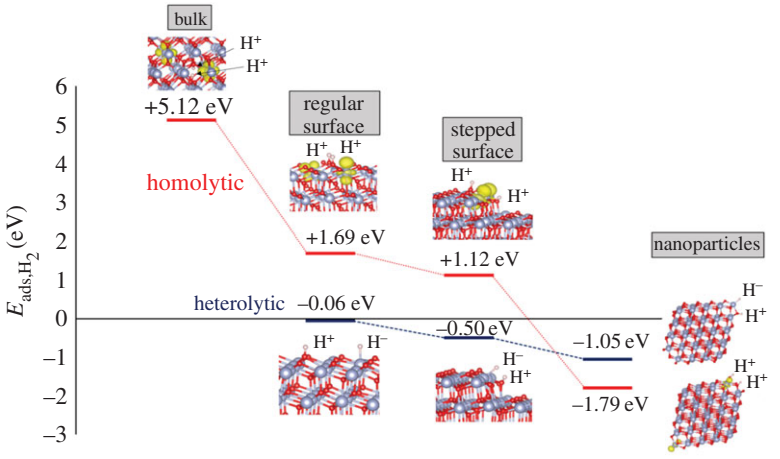

Figure 9. Energy change associated with the dissociation of H_2 on various models of ZrO_2. Red line: homolytic dissociation of H_2 (formation of two H^+ ions and two trapped e^- electrons). Blue line: heterolytic dissociation of H_2 (formation of H^+ and H^- ions). (Online version in colour.)

dissociation mechanism on highly ionic, non-reducible oxides. The reaction is slightly exothermic, with adsorption energy of −0.06 eV (figure 7). The H_2 homolytic splitting mechanism (formation of two O–H^+ bonds and reduction of two Zr^{4+} centres to Zr^{3+}) is endothermic by +1.69 eV. So, in the absence of defects, only the heterolytic splitting of H_2 is expected to occur on the extended ZrO_2(101) surface.

On the low-coordinated sites of the ZrO_2(156) stepped surface, the splitting into H^- and H^+ ions (heterolytic) is exothermic by −0.50 eV (more favourable compared to the regular terrace, where the gain is of −0.06 eV) [32]. The splitting into two H^+ ions and the subsequent reduction of the surface (formation of Zr^{3+} centres) is also more favourable at steps with respect to the regular terrace, but remains endothermic, with adsorption energy of +1.12 eV (figure 7*e*). There is a gain of about 0.6 eV going from the regular surface to the steps, but the heterolytic splitting remains by far the most favourable one. Thus, large crystallites of zirconia are not reduced by simple exposure to hydrogen (no direct formation of Zr^{3+} ions).

When the hydrogen molecule is adsorbed on zirconia nanoparticles, a different picture emerges. We considered next-neighbour corner sites (Zr–O or O–O sites) for the interaction with H_2, as these centres are expected to be more reactive. In $Zr_{80}O_{160}$, both H_2 dissociative mechanisms are exothermic, but the homolytic (reductive) one is the preferred dissociation path (−1.79 eV for homolytic versus −1.05 eV for heterolytic, figure 9). This is in contrast to what is observed on the extended surface. We observed the same behaviour also on the smaller nanoparticles. On $Zr_{16}O_{32}$ (0.9 nm) the homolytic splitting releases −1.62 eV while the heterolytic one is exothermic by −0.30 eV only. Different is the case of the nanoparticle of intermediate size, $Zr_{40}O_{80}$ (1.5 nm). This particle has an electronic structure in closer resemblance with the regular surface. Here, the two dissociation mechanisms are almost isoenergetic, $E_{ads} = -0.69$ eV (heterolytic) and $E_{ads} = -0.71$ eV (homolytic) [32]. To discard possible artefacts from the chosen DFT method, the order of stability of the two processes has been checked for the $Zr_{16}O_{32}$ nanoparticle by means of a DFT calculation using the more accurate PBE0 hybrid functional, but the trend does not change.

This is an important result. An opposite behaviour is found in dissociating H_2 when the extended zirconia surface is compared to zirconia nanoparticles of 2 nm in size. This can be explained with the peculiar electronic structure displayed by the zirconia nanoparticles. The presence of under-coordinated sites combined with quantum confinement effects introduces low-lying acceptor states in the band gap (e.g. fig. 4 in ref. [31]) that promote the formation of reduced

Zr^{3+} centres through a net charge transfer from H_2. That is, nanostructuring makes zirconia a reducible oxide, at variance with the bulk material.

6. Summary and conclusion

The catalytic conversion of lignocellulosic biomass in biofuels is a complex process consisting of various steps. The first one, pyrolysis, is followed by other steps where the biomass is upgraded by elongation of the C-chain and reduction of the oxygen content. Two key processes in this context are catalysed by metal oxides and consist in the transformation of carboxylic acids to ketones (ketonization), with the elimination of H_2O and CO_2, and deoxygenation, where phenol is transformed into benzene. Two oxides widely used in these processes are titania and zirconia. Although the oxide catalysts (ZrO_2, TiO_2, etc.) work also without any pre-treatment, there is evidence that a pre-treatment in hydrogen, with the reduction of the oxide, increases the catalytic activity.

The scope of this work is to rationalize the experimental observation of a larger activity of reducible compared to non-reducible oxides, and to identify the active sites that are generated in the course of the pre-treatment in hydrogen of the solid catalyst. To this end, we have performed extensive density functional theory calculations using the DFT + U approach to take into account the semiconductor/insulator nature of the oxides under investigation, TiO_2 and ZrO_2; we also included dispersion forces that are essential when organic molecules interact with a solid surface. Starting from the fact that the actual catalyst, at least at the laboratory scale, consists of Ru nanoparticles deposited on titania or zirconia, we have considered models of Ru aggregates supported on the (101) surfaces of anatase TiO_2 and tetragonal ZrO_2.

The first step consisted in the study of the two key processes in the upgrade of bio-oil: ketonization and DDO. In both cases, the behaviour of stoichiometric a-TiO_2 and t-ZrO_2 surfaces has been compared with that of the corresponding reduced counterparts, a-TiO_{2-x} and t-ZrO_{2-x}. Ketonization of acetic acid has been considered on the surface of ZrO_2, while deoxygenation of phenol has been studied on Ru/TiO_2. In both cases, we found evidence that the presence of Zr^{3+} or Ti^{3+} ions or of oxygen vacancies leads to lower reaction barriers or the stabilization of intermediates that have little or no stability on the stoichiometric surfaces.

Having established at a theoretical level that the reduction of the oxide enhances the activity of the catalyst, we have concentrated our attention on the mechanisms that can lead to a modification of the surface by chemical reduction. First, we demonstrated that the simple deposition of small Ru clusters on the surfaces of a-TiO_2 and t-ZrO_2 does not alter the electronic structure of the oxide. Despite some charge flow at the interface between the metal particle and the oxide (in particular for titania), there is no evidence of formation of reduced Ti^{3+} or Zr^{3+} centres. This is different from other metal–oxide interfaces, where the simple deposition of the metal results in a reduction of the support [28]. However, we have also shown that the presence of the metal particle favours the occurrence of the so-called oxygen reverse spillover. This consists in the migration of O atoms from the metal–oxide interface to the metal particle, with the formation of an oxygen vacancy and an adsorbed O atom on the metal cluster. This elementary process is the first step in the formation of an oxide overlayer on the top of the supported metal particle, sometimes referred to as 'strong metal support interaction'. According to our calculations, this process occurs with a very low thermodynamic cost and is more favourable on TiO_2 than on ZrO_2.

In the next step, we have considered the role of pre-treatment in H_2. H_2 does not dissociate on the surfaces of titania and zirconia. Furthermore, the process leads to different products: homolytic dissociation with the formation of two protons and two Ti^{3+} ions on titania (reducible oxide); and heterolytic dissociation with the formation of a proton adsorbed on O and a hydride ion adsorbed on Zr on zirconia (non-reducible oxide). The role of the supported metal particle, a Ru_{10} cluster in our case, is to split hydrogen in a non-activated exothermic process, leading to a hydrogenated Ru particle. The results show that at low hydrogen coverage the H atoms prefer to bind to the Ru particle, and do not diffuse to the oxide surface. Hydrogen spillover to the oxide only occurs after saturation coverage is reached, a limit where up to three H atoms per

Ru atom are adsorbed on the metal particle. The interesting aspect is that the species diffusing from the cluster to the oxide is a proton, but the associated electron follows this migration, leading to the final reduction of the oxide surface by hydrogen spillover (at least in the case of titania).

At this point, the surface becomes hydroxylated, with several OH groups present per surface unit. At the temperature usually adopted for biomass conversion, ≈5–600 K, water desorption can take place from the oxide surface, leaving behind the more reactive oxygen vacancy defect centres. This process is thermodynamically easier on titania than on zirconia, but the formation of vacancies corresponding to low-coordinated sites can occur at rather mild conditions even for zirconia.

This leads to the last aspect that we examined, the role of oxide nanostructuring. This analysis has been restricted to zirconia. In particular, zirconia nanoparticles containing up to 240 atoms ($Zr_{80}O_{160}$) have been studied in two processes: (i) reduction of the nanoparticles via oxygen vacancy formation by desorption of O_2; and (ii) reduction of the nanoparticles via H_2 addition. In the first case, the results show that, while the creation of an oxygen vacancy at the surface of ZrO_2 is energetically very unfavourable (the cost is the same as in the bulk), low-coordinated O atoms at exposed sites of the nanoparticles are much easier to remove. Even more surprising are the results for H_2 treatment. While on the zirconia surface H_2 can only dissociate heterolytically, with the formation of H^+ and H^- ions and no reduction of the surface (no formation of Zr^{3+} centres), on ZrO_2 nanoparticles the dissociation becomes exothermic and, more important, homolytic, with the formation of two protons and two trapped electrons in 4d states of Zr ions (formation of Zr^{3+}). In this respect, the zirconia nanoparticles behave as bulk titania, turning the non-reducible ZrO_2 into a reducible oxide.

Overall, the study provides an atomistic view of the processes of oxide reduction and a rationalization of the importance of generating reduced oxide surfaces in two technologically important reactions such as ketonization and DDO. The general concepts and notions reported, however, are applicable to any class of reactions where oxide surfaces are involved and where the reducibility of the support plays an active role in the reaction.

Data accessibility. This article has no additional data.

Authors' contribution. S.T., H.Y.T.C. and A.R.P. carried out the computational work, participated in data analysis, and contributed to the design of the study and to drafting part of the manuscript; G.P. conceived and designed the study, coordinated the work and helped draft the manuscript. All authors gave final approval for publication.

Competing interests. We declare we have no competing interests.

Funding. This work has been supported by the European Community's Seventh Framework Programme FP7/2007-2013 under Grant Agreement no. 604307 (CASCATBEL), the European Marie Curie Network CATSENSE (Grant Agreement no. 607417), and by Italian MIUR through the PRIN Project 2015K7FZLH SMARTNESS 'Solar driven chemistry: new materials for photo- and electro-catalysis'.

Acknowledgment. We acknowledge the support of the Regione Lombardia and Italian CINECA Supercomputing Centre via the LISA Joint Initiative, Project HPL13PKBV5.

References

1. Barteau MA. 1996 Oxygen reactions at well-defined oxide surfaces. *Chem. Rev.* **96**, 1413–1430. (doi:10.1021/cr950222t)
2. Mohan D, Pittman CU, Steele PH. 2006 Pyrolysis of wood/biomass for bio-oil: a critical review. *Energy Fuels* **20**, 848–889. (doi:10.1021/ef0502397)
3. Shen WQ, Tompsett GA, Xing R, Conner WC, Huber GW. 2012 Vapor phase butanal self-condensation over unsupported and supported alkaline earth metal oxides. *J. Catal.* **286**, 248–259. (doi:10.1016/j.jcat.2011.11.009)
4. Faba L, Díaz F, Ordóñez S. 2014 One-pot aldol condensation and hydrodeoxygenation of biomass-derived carbonyl compounds for biodiesel synthesis. *ChemSusChem* **7**, 2816–2820. (doi:10.1002/cssc.201402236)

5. Kikhtyanin O, Kubicka D, Cejka J. 2015 Toward understanding of the role of Lewis acidity in aldol condensation of acetone and furfural using MOF and zeolite catalysts. *Catal. Today* **243**, 158–162. (doi:10.1016/j.cattod.2014.08.016)
6. Rajadurai S. 1994 Pathways for carboxylic acid decomposition on transition metal oxides. *Catal. Rev.* **36**, 385–403. (doi:10.1080/01614949408009466)
7. Martinez R, Huff MC, Barteau MA. 2004 Ketonization of acetic acid on titania-functionalized silica monoliths. *J. Catal.* **222**, 404–409. (doi:10.1016/j.jcat.2003.12.002)
8. Pham TN, Sooknoi T, Crossley SP, Resasco DE. 2013 Ketonization of carboxylic acids: mechanisms, catalysts, and implications for biomass conversion. *ACS Catal.* **3**, 2456–2473. (doi:10.1021/cs400501h)
9. Pacchioni G. 2014 Ketonization of carboxylic acids in biomass conversion over TiO_2 and ZrO_2 surfaces: a DFT perspective. *ACS Catal.* **4**, 2874–2888. (doi:10.1021/cs500791w)
10. Wang S, Iglesia E. 2017 Experimental and theoretical assessment of the mechanism and site requirements for ketonization of carboxylic acids. *J. Catal.* **345**, 183–206. (doi:10.1016/j.jcat.2016.11.006)
11. Nelson RC, Baek B, Ruiz P, Goundie B, Brooks A, Wheeler MC, Frederick BG, Grabow LC, Austin RN. 2015 Experimental and theoretical insights into the hydrogen-efficient direct hydrodeoxygenation mechanism of phenol over Ru/TiO_2. *ACS Catal.* **5**, 6509–6523. (doi:10.1021/acscatal.5b01554)
12. Newman C *et al.* 2014 Effects of support identity and metal dispersion in supported ruthenium hydrodeoxygenation catalysts. *Appl. Catal. A Gen.* **477**, 64–74. (doi:10.1016/j.apcata.2014.02.030)
13. Mortensen PM, Grunwaldt JD, Jensen PA, Jensen AD. 2013 Screening of catalysts for hydrodeoxygenation of phenol as a model compound for bio-oil. *ACS Catal.* **3**, 1774–1785. (doi:10.1021/cs400266e)
14. Pham TN, Shi D, Resasco DE. 2014 Reaction kinetics and mechanism of ketonization of aliphatic carboxylic acids with different carbon chain lengths over Ru/TiO_2 catalyst. *J. Catal.* **314**, 149–158. (doi:10.1016/j.jcat.2014.04.008)
15. Pham TN, Shi D, Resasco DE. 2014 Kinetics and mechanism of ketonization of acetic acid on Ru/TiO_2 catalyst. *Top. Catal.* **57**, 706–714. (doi:10.1007/s11244-013-0227-7)
16. Pham TN, Shi D, Sooknoi T, Resasco DE. 2012 Aqueous-phase ketonization of acetic acid over Ru/TiO_2/carbon catalysts. *J. Catal.* **295**, 169–178. (doi:10.1016/j.jcat.2012.08.012)
17. Foraita S, Fulton JL, Chase ZA, Vjunov A, Xu P, Baráth E, Camaioni DM, Zhao C, Lercher JA. 2015 Impact of the oxygen defects and the hydrogen concentration on the surface of tetragonal and monoclinic ZrO_2 on the reduction rates of stearic acid on Ni/ZrO_2. *Chem. Eur. J.* **21**, 2423–2434. (doi:10.1002/chem.201405312)
18. Okumura K, Iwasawa Y. 1996 Zirconium oxides dispersed on silica derived from Cp_2ZrCl_2, $[(i\text{-}PrCp)_2ZrH(\mu\text{-}H)]_2$, and $Zr(OEt)_4$ characterized by X-ray absorption fine structure and catalytic ketonization of acetic acid. *J. Catal.* **164**, 440–448. (doi:10.1006/jcat.1996.0400)
19. Panchenko VN, Zaytseva YA, Simonov MN, Simakova IL, Paukshtis EA. 2014 DRIFTS and UV-vis DRS study of valeric acid ketonization mechanism over ZrO_2 in hydrogen atmosphere. *J. Mol. Catal. A Chem.* **388–389**, 133–140. (doi:10.1016/j.molcata.2013.11.012)
20. Ignatchenko AV, Kozliak EI. 2012 Distinguishing enolic and carbonyl components in the mechanism of carboxylic acid ketonization on monoclinic zirconia. *ACS Catal.* **2**, 1555–1562. (doi:10.1021/cs3002989)
21. Pulido A, Oliver-Tomas B, Renz M, Boronat M, Corma A. 2013 Ketonic decarboxylation reaction mechanism: a combined experimental and DFT study. *ChemSusChem* **6**, 141–151. (doi:10.1002/cssc.201200419)
22. Lee Y, Choi J-W, Suh DJ, Ha J-M, Lee CH. 2015 Ketonization of hexanoic acid to diesel-blendable 6-undecanone on the stable zirconia aerogel catalyst. *Appl. Catal. A* **506**, 288–293. (doi:10.1016/j.apcata.2015.09.008)
23. Ignatchenko AV, DeRaddo JS, Marino VJ, Marino A, Mercado A. 2015 Cross-selectivity in the catalytic ketonization of carboxylic acids. *Appl. Catal. A* **498**, 10–24. (doi:10.1016/j.apcata.2015.03.017)
24. Peng B, Zhao C, Kasakov S, Foraita S, Lercher JA. 2013 Manipulating catalytic pathways: deoxygenation of palmitic acid on multifunctional catalysts. *Chem. Eur. J.* **19**, 4732–4741. (doi:10.1002/chem.201203110)

25. Tosoni S, Pacchioni G. 2016 Acetic acid ketonization on tetragonal zirconia: role of surface reduction. *J. Catal.* **344**, 465–473. (doi:10.1016/j.jcat.2016.10.002)
26. Chen H-Y, Pacchioni G. 2016 Role of oxide reducibility in the deoxygenation of phenol on rutheniun clusters supported on the anatase TiO_2 (101) surface. *ChemCatChem* **8**, 2492–2499. (doi:10.1002/cctc.201600457)
27. Chen H-Y, Tosoni S, Pacchioni G. 2014 Adsorption of ruthenium atoms and clusters on anatase TiO_2 and tetragonal ZrO_2 (101) surfaces: a comparative DFT study. *J. Phys. Chem. C* **119**, 10 856–10 868. (doi:10.1021/jp510468f)
28. Pacchioni G. 2013 Electronic interactions and charge transfers of metal atoms and clusters on oxide surfaces. *Phys. Chem. Chem. Phys.* **15**, 1737–1757. (doi:10.1039/c2cp43731g)
29. Chen H-Y, Tosoni S, Pacchioni G. 2015 Hydrogen adsorption, dissociation, and spillover on Ru_{10} clusters supported on anatase TiO_2 and tetragonal ZrO_2 (101) surfaces. *ACS Catal.* **5**, 5486–5495. (doi:10.1021/acscatal.5b01093)
30. Gionco C, Paganini MC, Giamello E, Burgess R, Di Valentin C, Pacchioni G. 2013 Paramagnetic defects in polycrystalline zirconia: an EPR and DFT study. *Chem. Mater.* **25**, 2243–2253. (doi:10.1021/cm400728j)
31. Ruiz Puigdollers A, Illas F, Pacchioni G. 2016 Structure and properties of zirconia nanoparticles from density functional theory calculations. *J. Phys. Chem. C* **120**, 4392–4402. (doi:10.1021/acs.jpcc.5b12185)
32. Ruiz Puigdollers A, Tosoni S, Pacchioni G. 2016 Turning a nonreducible into a reducible oxide via nanostructuring: opposite behavior of bulk ZrO_2 and ZrO_2 nanoparticles towards H_2 adsorption. *J. Phys. Chem. C* **120**, 15 329–15 337. (doi:10.1021/acs.jpcc.6b05984)
33. Kresse G, Furthmüller J. 1996 Efficiency of ab-initio total energy calculations for metals and semiconductors using a plane-wave basis set. *J. Comput. Mater. Sci.* **6**, 15–50. (doi:10.1016/0927-0256(96)00008-0)
34. Perdew JP, Burke K, Ernzerhof M. 1996 Generalized gradient approximation made simple. *Phys. Rev. Lett.* **77**, 3865–3868. (doi:10.1103/PhysRevLett.77.3865)
35. Anisimov VI, Zaanen J, Andersen OK. 1991 Band theory and Mott insulators: Hubbard *U* instead of Stoner *I*. *Phys. Rev. B* **44**, 943–954. (doi:10.1103/PhysRevB.44.943)
36. Dudarev SL, Botton GA, Savrasov SY, Humphreys CJ, Sutton AP. 1998 Electron-energy-loss spectra and the structural stability of nickel oxide: an LSDA+U study. *Phys. Rev. B* **57**, 1505–1509. (doi:10.1103/PhysRevB.57.1505)
37. Grimme S. 2006 Semiempirical GGA-type density functional constructed with a long-range dispersion correction. *J. Comput. Chem.* **27**, 1787–1799. (doi:10.1002/jcc.20495)
38. Ruiz Puigdollers A, Schlexer P, Pacchioni G. 2015 Gold and silver clusters on TiO_2 and ZrO_2 (101) surfaces: role of dispersion forces. *J. Phys. Chem. C* **119**, 15 381–15 389. (doi:10.1021/acs.jpcc.5b04026)
39. Blöchl PE. 1994 Projector augmented-wave method. *Phys. Rev. B* **50**, 17 953–17 979. (doi:10.1103/PhysRevB.50.17953)
40. Kresse G, Joubert J. 1999 From ultrasoft pseudopotentials to the projector augmented-wave method. *Phys. Rev. B* **59**, 1758–1775. (doi:10.1103/PhysRevB.59.1758)
41. Neunhoeffer O, Paschke P. 1939 Über den Mechanismus der Ketonbildung aus Carbonsäuren. *Ber. Dtsch. Chem. Ges. A/B* **72**, 919–929. (doi:10.1002/cber.19390720442)
42. Ignatchenko AV. 2011 Density functional theory study of carboxylic acids adsorption and enolization on monoclinic zirconia surfaces. *J. Phys. Chem. C* **115**, 16 012–16 018. (doi:10.1021/jp203381h)
43. McComb DW. 1996 Bonding and electronic structure in zirconia pseudopolymorphs investigated by electron energy-loss spectroscopy. *Phys. Rev. B* **54**, 7094–7102. (doi:10.1103/PhysRevB.54.7094)
44. Shutilov AA, Simonov MN, Zaytseva YA, Zenkovets GA, Simakova IL. 2013 Phase composition and catalytic properties of ZrO_2 and CeO_2–ZrO_2 in the ketonization of pentanoic acid to 5-nonanone. *Kinet. Catal.* **54**, 184–192. (doi:10.1134/S0023158413020134)
45. Zaytseva YA, Panchenko VN, Simonov MN, Shutilov AA, Zenkovets GA, Renz M, Simakova IL, Parmon VN. 2013 Effect of gas atmosphere on catalytic behaviour of zirconia, ceria and ceria–zirconia catalysts in valeric acid ketonization. *Top. Catal.* **56**, 846–855. (doi:10.1007/s11244-013-0045-y)

46. Li CM *et al.* 2013 Photohole-oxidation-assisted anchoring of ultra-small Ru clusters onto TiO_2 with excellent catalytic activity and stability. *J. Mater. Chem. A* **1**, 2461–2467. (doi:10.1039/c2ta01205g)
47. Zhang S-T, Li C-M, Yan H, Wei M, Evans DG, Duan X. 2014 Density functional theory study of metal–support interaction between Ru cluster and anatase TiO_2(101) surface. *J. Phys. Chem. C* **118**, 3514–3522. (doi:10.1021/jp409627p)
48. Bredow T, Aprà E, Catti M, Pacchioni G. 1998 Cluster and periodic calculations on K/TiO_2(110). *Surf. Sci.* **418**, 150–165. (doi:10.1016/S0039-6028(98)00712-2)
49. Luches P, Pagliuca F, Valeri S, Illas F, Preda G, Pacchioni G. 2012 Nature of Ag islands and nanoparticles on the CeO_2 (111) surface. *J. Phys. Chem. C* **116**, 1122–1132. (doi:10.1021/jp210241c)
50. Pacchioni G, Pescarmona P. 1998 Structure and stability of oxygen vacancies on sub-surface, terraces, and low-coordinated surface sites of MgO: an ab initio study. *Surf. Sci.* **412–413**, 657–671. (doi:10.1016/S0039-6028(98)00501-9)
51. Pacchioni G, Freund H. 2013 Electron transfer at oxide surfaces. The MgO paradigm: from defects to ultrathin films. *Chem. Rev.* **113**, 4035–4072. (doi:10.1021/cr3002017)
52. Prins R. 2012 Hydrogen spillover. Facts and fiction. *Chem. Rev.* **112**, 2714–2738. (doi:10.1021/cr200346z)
53. Karim W, Spreafico C, Kleibert A, Gobrecht J, VandeVondele J, Ekinci Y, van Bokhoven J. 2017 Catalyst support effects on hydrogen spillover. *Nature* **541**, 68–73. (doi:10.1038/nature20782)
54. Vayssilov GN, Gates BC, Rösch N. 2003 Oxidation of supported rhodium clusters by support hydroxy Groups. *Angew. Chem. Int. Ed.* **42**, 1391–1394. (doi:10.1002/anie.200390357)
55. Ivanova Shor EA, Nasluzov VA, Shor AM, Vayssilov GN, Rösch N. 2007 Reverse hydrogen spillover onto zeolite-supported metal clusters: an embedded cluster density functional study of models M_6 (M = Rh, Ir, or Au). *J. Phys. Chem. C* **111**, 12 340–12 351. (doi:10.1021/jp0711287)
56. Hu CH, Chizallet C, Mager-Maury C, Corral-Valero M, Sautet P, Toulhoat H, Raybaud P. 2010 Modulation of catalyst particle structure upon support hydroxylation: ab initio insights into Pd_{13} and Pt_{13}/γ-Al_2O_3. *J. Catal.* **274**, 99–110. (doi:10.1016/j.jcat.2010.06.009)
57. Mager-Maury C, Chizallet C, Sautet P, Raybaud P. 2012 Platinum nanoclusters stabilized on γ-alumina by chlorine used as a capping surface ligand: a density functional theory study. *ACS Catal.* **2**, 1346–1357. (doi:10.1021/cs300178y)
58. Keren E, Soffer A. 1977 Simultaneous electronic and ionic surface conduction of catalyst supports: a general mechanism for spillover: the role of water in the Pd-catalyzed hydrogenation of a carbon surface. *J. Catal.* **50**, 43–55. (doi:10.1016/0021-9517(77)90007-0)
59. Chen H-Y, Giordano L, Pacchioni G. 2013 From heterolytic to homolytic H_2 dissociation on nanostructured MgO(001) films as a function of the metal support. *J. Phys. Chem. C* **117**, 10 623–10 629. (doi:10.1021/jp4037588)
60. Jensen C, Buck D, Dilger H, Bauer M, Phillipp F, Roduner E. 2013 Maximum hydrogen chemisorptions on KL zeolite supported Pt clusters. *Chem. Commun.* **49**, 588–590. (doi:10.1039/C2CC37933C)
61. Islam MM, Calatayud M, Pacchioni G. 2011 Hydrogen adsorption and diffusion on the anatase TiO_2(101) surface: a first-principles investigation. *J. Phys. Chem. C* **115**, 6809–6814. (doi:10.1021/jp200408v)
62. Panayotov DA, Yates Jr JT. 2007 Spectroscopic detection of hydrogen atom spillover from Au nanoparticles supported on TiO_2: use of conduction band electrons. *J. Phys. Chem. C* **111**, 2959–2964. (doi:10.1021/jp066686k)
63. Redhead PA. 1962 Thermal desorption of gases. *Vacuum* **12**, 203–211. (doi:10.1016/0042-207X(62)90978-8)
64. Christmann K. 1991 *Introduction to surface physical chemistry*, p. 156. Berlin, Germany: Springer.